Journal of Physics and Chemistry of Solids 74 (2013) 205–214

Contents lists available at SciVerse ScienceDirect

Journal of Physics and Chemistry of Solids

journal homepage: www.elsevier.com/locate/jpcs

Mechanical properties of bulk and nanostructured $La_{0.61}Sr_{0.39}MnO_3$ perovskite manganite materials

P. Kulandaivelu [a], K. Sakthipandi [c], P. Senthil Kumar [b], V. Rajendran [c,*]

[a] Mechanical Engineering, K S Rangasamy College of Technology, Tiruchengode 637 215, Tamil Nadu, India
[b] Department of Mechanical Engineering, K S R College of Engineering, Tiruchengode 637 215, Tamil Nadu, India
[c] Centre for Nano Science and Technology, K S Rangasamy College of Technology, Tiruchengode 637215, Tamil Nadu, India

ARTICLE INFO

Article history:
Received 2 December 2011
Received in revised form
30 July 2012
Accepted 19 September 2012
Available online 27 September 2012

Keywords:
A. Magnetic materials
B. Chemical synthesis
C. Ultrasonic measurements
D. Elastic properties
D. Phase transitions

ABSTRACT

Ultrasonic non-destructive measurement is a versatile and sensitive tool for evaluating the mechanical properties of solids. $La_{0.61}Sr_{0.39}MnO_3$ perovskite magnetic material in bulk and at nanoscale was prepared by solid-state reaction and sonochemical reactor methods, respectively. Evaluation of the mechanical properties of the prepared bulk and nano samples was made through on-line ultrasonic velocity measurements over a wide range of temperature from 300 to 400 K. The observed anomalous behaviour in elastic moduli was used to explore the phase transition temperature (Curie temperature T_C), that is, from paramagnetic (PM) to ferromagnetic (FM) phase, both in bulk and nanostructured perovskite samples. Further, the behaviour of phase transition both in bulk and nano perovskites was explored through the observed anomalous behaviour.

1. Introduction

The magnetotransport and magnetic properties of $La_{1-x}Sr_xMnO_3$ (LSMO) perovskites have received attention in recent years because of the colossal magnetoresistance (CMR) effect in its ferromagnetic phase (FM) [1–3]. The doping of Sr in place of La leads to a gradual change from antiferromagnetic insulating (AFI) ground state to ferromagnetic metallic (FMM) phase because of progressive increase in the number of holes from Mn^{3+} to Mn^{4+}. The existence of the observed CMR near transition temperature was due to the mixed valence state of Mn, evolving from Mn^{3+} (Spin S=2) in the parent atom $LaMnO_3$ to Mn^{4+} (Spin S=3/2) to the doped element $SrMnO_3$ [4–5]. The double exchange interaction of the neighbouring spin moment of Mn^{3+}/Mn^{4+} coupled through oxygen ions was used to explain the CMR phenomenon near the transition temperature [6,7]. In addition, the small polaron theory and the Jahn–Teller (JT) effect have been proposed to explain the CMR effect. Strontium-doped $LaMnO_3$ was considered to be a very attractive electrolyte for moderate temperatures (600–900 K) because of its relatively high ionic conductivity and chemical stability with low carrier concentration density and a high spin polarisation of the charge carrier [8–9].

$La_{0.61}Sr_{0.39}MnO_3$ perovskite materials possess a higher Curie temperature (T_C), which makes it very promising for room temperature applications like in actuators, switches, magnetic field sensors, and electronic devices [6–7]. Thus, it is interesting to explore the influence of particle size on the exotic properties of perovskite magnetic materials. The enhancement in the optical, resistivity, thermal and magnetic properties of materials by reduction in particle sizes is well proven in nanostructured materials. The nanostructured materials are used to widen the opportunities to improve the catalytic activity in solid fuel cells [7]. Physical concepts such as Zener double exchange (ZDE) [3,4] and the Jahn–Teller (JT) effect [8,9] have been used to explain phenomena like CMR and dense granular magnetoresistance (GMR).

Perovskite manganite materials reveal an interesting magnetic and electronic property across compositional and temperature ranges. These existing complex phase diagrams and interesting physical properties of manganite materials have been characterised using complex interplay and interaction/competition of lattice, spin, orbital, and strain degrees of freedom, which are coupled strongly to each other [10–13]. The LSMO systems offer a degree of chemical flexibility that permits the relationship between the structural, electronic, and magnetic properties of perovskites to be examined in a systematic manner [14].

In recent years, the synthesis and characterisation of nanostructured perovskites have been a fascinating topic with size-dependent optical, electronic, magnetic, thermal, mechanical, and chemical properties [15–17]. Nanoscale materials possess intriguing properties that are comparable to or superior to those of bulk perovskites, leading to potential applications in areas like

* Corresponding author. Tel.: +91 4288 274 741 4; fax: +91 4288 274 870.
E-mail address: veerajendran@gmail.com (V. Rajendran).

0022-3697/$ - see front matter © 2012 Elsevier Ltd. All rights reserved.
http://dx.doi.org/10.1016/j.jpcs.2012.09.008

energy storage, fuel cells, nanomedicine, molecular computing, nanophotonics tunable resonant devices, catalysts, and sensors [18,19].

In mixed valent manganites, the electronic properties are closely related to the lattice. Many of the interesting phenomena exhibited by them involve a complex interplay between the structural, spin, charge, and orbital degrees of freedom, accompanied with subtle displacements in the crystal lattice. The measured ultrasonic parameters such as ultrasonic velocities and attenuation are more sensitive with lattice/structure and hence used to explore the displacement of lattices. In addition, the measured ultrasonic parameters are influenced by many desired parameters like rigidity modulus, bulk modulus, Young's modulus, internal friction, thermal expansion, etc. [20–21]. Thus, on-line ultrasonic measurements were successfully used to obtain the elastic constants of the manganite perovskite [21].

The aim of the present study was to synthesise and understand the structural and physical properties of $La_{0.61}Sr_{0.39}MnO_3$ perovskites both in their bulk and nanoscale state. It also aimed to explore the structural and physical property changes during the transformation from bulk to nano phase.

2. Experimental

2.1. Sample preparation

The nominal composition of bulk and nanostructured $La_{0.61}Sr_{0.39}MnO_3$ perovskites comprised lanthanum nitrate (99.999%, Sigma Aldrich), manganese carbonate (99.9%, Sigma Aldrich), and strontium nitrate (99.0%, Himedia GR) powders as starting materials. To prepare the bulk sample, the stoichiometric ratio of the starting materials was mixed in an agate mortar. The mixture was calcinated at 873 K twice in air for 2 h using solid-state reaction. To prepare the nano sample, initially, manganese carbonate was sonicated in dilute nitric acid for 20 min to convert the insoluble carbonate into soluble nitrate. A highly intense sonication was carried out at a constant temperature of 353 K with titanium horn operated at a frequency of 20 kHz (Sonics, USA). During the sonication process, lanthanum nitrate and strontium nitrate salt solutions were added to the manganese solution. The pH value of the solution was adjusted to ~7 after the sonication. Later, the solution was allowed to dry in a hot air oven at a constant temperature of 393 K for 24 h. The black residue formed was collected and then calcined in air at 873 K for 2 h. Thereafter, the calcined bulk and nano perovskite powders were pressed separately into a pellet and sintered at 1273 K for 12 h in atmospheric air. The sintered pellets were used for further characterisation studies.

2.2. X-ray diffractometry

The crystalline nature and crystallite size of the bulk and nano perovskite manganite samples were obtained by recording X-ray diffraction (XRD) patterns using a powder X-ray diffractometer (X' Pert Pro, Analytical, Netherland). The XRD patterns were obtained using CuK_α as a radiation source with an operating voltage of 40 kV and a current rating of 30 mA. The XRD pattern was obtained in the scan range of 10–80° with an increment of 0.05°. By knowing the full-width at half-maximum ($\beta_{1/2}$) and the angle of diffraction (θ) of the XRD peaks, the average particle size (D_{XRD}) of both samples was obtained using Scherrer's equation [22]:

$$D_{XRD} = \frac{0.94\lambda}{\beta_{1/2}\cos\theta} \quad (1)$$

where λ ($=1.5406$ A°) is the wavelength of the CuK_α source used in X-ray radiation.

2.3. Density

Using the Archimedes principle, the mass density of the bulk and nano perovskite samples was measured by weighing the sample in air (W_a) and CCl_4 buoyant (W_b). The density of the sample was obtained as follows:[19,20]

$$\rho = \frac{W_a}{W_a - W_b}\rho_b \quad (2)$$

where ρ_b is the density of buoyant. The experiment was repeated five times, and the average value was taken as the density of the sample. The percentage error in the measurement of density was ± 0.05.

2.4. Microscopy

A scanning electron microscope (SEM) coupled with energy-dispersive analysis of X-ray (EDAX) (JEOL, JSM 5300) was used to obtain the surface images of the bulk and nano perovskite manganite samples to explore the morphology, microstructure, and composition of the perovskite samples. The substructural information and particle size of the samples were obtained from TEM images using a transmission electron microscope (TEM, Philips, CM 200, USA).

2.5. Fourier transformation infrared spectroscopy

Fourier transformation infrared absorption spectra (FTIR) of both bulk and nano perovskite samples were recorded at room temperature from wave number 4000–400 cm^{-1} with a resolution of 1 cm^{-1} (20 scans) using a spectrometer (Spectrum 100, PerkinElmer, USA). The recorded FTIR spectra were used to reveal the functional group of the bulk and nano perovskite samples. The required sample (2.0 mg) was mixed with 200 mg of KBr in an agate mortar. Thereafter, the mixture powder was pelleted into a pellet of 13-mm diameter with a thickness of 0.2 mm for FTIR measurement. The blank KBr pellet was used to normalise the FTIR spectrum.

2.6. Surface area analysis

The specific surface area (S_{BET}) of both bulk and nano perovskite samples was determined using a Brunauer–Emmett–Teller (BET) surface area analyser (Autosorb-1, Quantachrome, USA) using the nitrogen adsorption–desorption method. Before starting the measurement, the sample was degassed at 463 K for 3 h to remove physically absorbed gas molecules and moisture. The measured specific surface area and density (ρ) of the bulk and nano perovskite manganites were used to obtain the equivalent spherical diameter (D_{BET}) of bulk and nano perovskite samples using the following formula: [23]

$$D_{BET} = \frac{6}{\rho S_{BET}} \quad (3)$$

2.7. Ultrasonic velocities measurement

The through transmission technique was used to measure ultrasonic velocity as a function of temperature from 300 to 400 K [20]. A high-power ultrasonic Pulser Receiver (Olympus NDT, 5900 PR, USA) was used for transmission and reception of ultrasonic signals, and a computer in-built 1-GHz digital storage oscilloscope (DSO) (Lecroy, Wave Runner 104 MXi, USA) was used to record digital ultrasonic (rf) signals. X- and Y-cut transducers operating at a fundamental frequency of 5 MHz were used for

generation of longitudinal and shear waves, respectively. As discussed earlier [20], an indigenously designed experimental set-up was used to measure the ultrasonic velocities over a wide range of temperature. Using a programmable temperature controller (Eurotherm, 2604, USA), the sample temperature was heated from 300 to 400 K at a heating rate of 0.5 K min^{-1}. The error in the measurement of temperature was ± 1 K. Elastic constants such as longitudinal modulus ($L=U_L^2\rho$), shear modulus ($G=U_S^2\rho$), bulk modulus ($K=L-(4/3)G$), Possion's ratio ($\sigma=(L-2G)/2(L-G)$), and Young's modulus ($E=(1+\sigma)$ 2G) were obtained utilising the measured velocities and density using standard formulae [20].

3. Results and discussion

The obtained XRD patterns of both bulk and nano $La_{0.61}Sr_{0.39}MnO_3$ perovskite manganite samples shown in Fig. 1 reveal the crystalline nature. In XRD patterns, the observed peaks were narrow in bulk LSMO samples, whereas it was broad in the case of nano LSMO perovskites. The observed diffracted peaks of bulk samples at planes (011), (202), (024) (030), and (220) and the diffracted peaks of nano perovskite samples at planes (012), (011), (012), (202), (006), (024), (122), (030), (220), (208), and (134) confirm the rhombohedral structure with R3c space group (JCPDS file no.: 51-0409 and 51-0118). The above information shows that both the prepared bulk and nano LSMO samples were in crystalline nature as reported elsewhere [24–25]. In addition to the structural information obtained from XRD patterns, an intensity observation, that is, the shifting of the diffraction angle (2θ) to a lower value in nanosamples compared with bulk samples was obtained.

The observed broadening of peaks in the XRD patterns can be attributed to the nanocrystalline nature of the prepared nano samples. For example, the rhombohedral peak observed at plane (110) is broad in area in the case of nano LSMO compared with bulk LSMO perovskite samples. In addition, the observed diffraction angle (2θ) is shifted towards a lower value in nano LSMO samples (32.6°) compared with bulk LSMO (32.9°) samples. Scherrer's equation was used to obtain the crystallite size of both bulk and nano LSMO samples, which are, respectively, 0.459 μm and 32 nm. A similar peak broadening effect and shifting of peaks for nano crystalline perovskite samples were observed in our earlier studies [20].

The FTIR spectra of both bulk and nano $La_{0.61}Sr_{0.39}MnO_3$ perovskite manganite samples are shown in Fig. 2. The different functional groups existing in both bulk and nano LSMO perovskite samples were analysed using FTIR spectra. The spectra show a broad peak in the low wave number range of 450–600 cm^{-1}, which can be ascribed to Mn–O and O–Mn–O bonds due to the Jahn–Teller effect [26]. The functional group corresponding to the stretching and bending mode of the OH bond of water was reflected in the FTIR spectra at 3400 and 1630 cm^{-1}, respectively [27–28]. Further, the bands corresponding to the impurity phase $SrCO_3$ and CH_3 or CH_2 coupled with OH bands were reflected in small peaks at 2900 cm^{-1}. However, the actual finger prints of the prepared bulk and nano samples were reflected in the wavenumber 400–2000 cm^{-1}. The observed band frequencies and their corresponding assignment of the functional groups are given in Table 1.

Fig. 3 reveals compositional analysis (EDX) of both bulk and nano $La_{0.61}Sr_{0.39}MnO_3$ perovskite manganite samples. It can be observed from the EDX spectra that both bulk and nano perovskite samples are composed of La, Ca, Mn, and O atoms. The molar ratio for the elements La, Sr, Mn, and O was obtained from the EDX spectra as shown in Fig. 3. The molar ratio of elements La, Sr, Mn and O were respectively 0.61, 0.39, 1 and 2.99 in the bulk LSMO sample, and 0.615, 0.395, 1 and 3 in the nano LSMO samples. It was clear from EDX measurement that the atomic ratio of elements La, Sr, Mn and O atoms are in close agreement with that of the nominal composition of bulk and nano $La_{0.61}Sr_{0.39}MnO_3$ perovskite samples. Thus, the above studies confirm the absence of impurities in both bulk and nano LSMO perovskite samples.

Figs. 4–6 reveal the microstructure/morphology (SEM), particle size (TEM) and selected area electron diffraction (SAED) of both bulk and nano $La_{0.61}Sr_{0.39}MnO_3$ perovskite manganite samples. Further, SEM and TEM measurements were carried out in the recovered sample after temperature dependent ultrasonic measurement. The approximate particle size determined from SEM images of bulk and nano samples by considering the minimum and maximum diameter of a large number of particles is given in Table 1. The SEM images of bulk and nano perovskite samples show that the particles are agglomerated with spherical-like

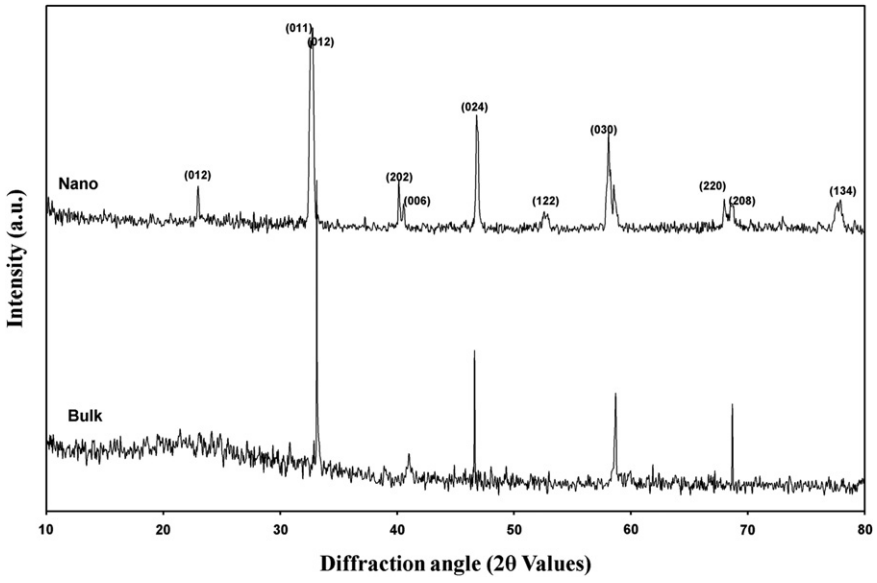

Fig. 1. XRD pattern of bulk and nano $La_{0.61}Sr_{0.39}MnO_3$ perovskite manganite materials.

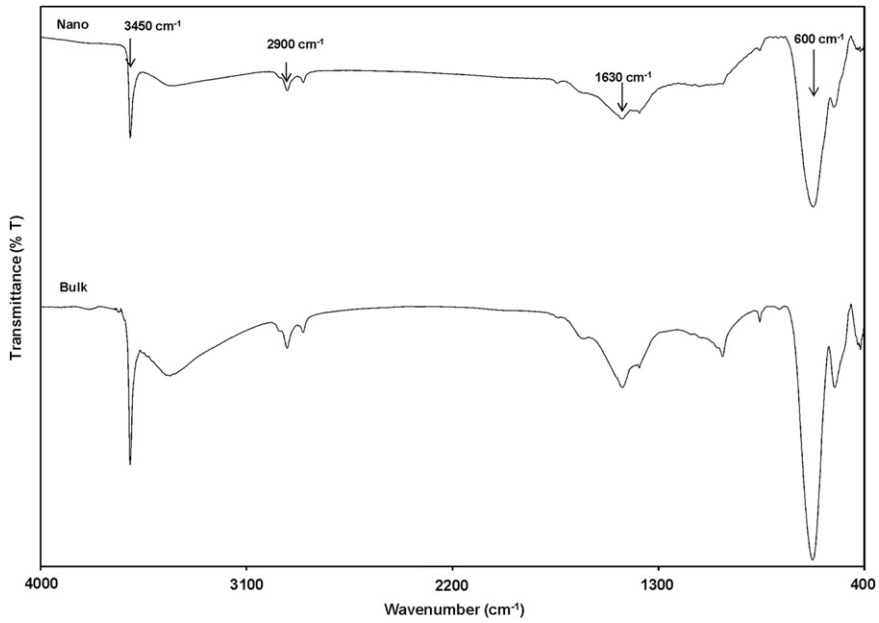

Fig. 2. FTIR spectrum of bulk and nano $La_{0.61}Sr_{0.39}MnO_3$ perovskite manganite materials.

Table 1
Investigations on variation of nano LSMO from its bulk properties.

Studies		Parameter	Bulk	Nano
XRD		Grain size	0.459 ± 0.01 μm	32 ± 3 nm
FTIR		Wavenumber (cm^{-1})	Functional group assignments	
		450–600	Stretching mode of Mn–O	
		1630	H–O–H bending mode	
		3400	O–H stretching mode	
BET		Equivalent spherical diameter	416 ± 4 μm	27 ± 4 nm
SEM	Before heat treatment	Particle size	0.65 ± 0.07 μm	60 ± 0.05 nm
	After heat treatment		0.75 ± 0.05 μm	$90–120 \pm 5$ nm
TEM	Before heat treatment	Particle size	0.6 ± 0.05 μm	$30–60 \pm 5$ nm
	After heat treatment		0.7 ± 0.05 μm	$50–80 \pm 5$ nm
Ultrasonic studies		Anomalous region	366–370 K	354–379 K
		Transition temperature	368 K	361 K

morphology consisting of agglomerated particles with indefinite boundaries. A detailed and clear morphology for the bulk and nano perovskite samples, along with their particle size, can be obtained from the TEM (Fig. 5) images. It is interesting to note from TEM studies that as-prepared nano perovskite samples assumed a honeycomb structure with different sizes of nano particles in the range from 30 to 60 nm.

Further, the particles were little agglomerated, which is evident from SEM and TEM measurements due to higher reaction temperature, longer heating time and high homogenousity in nature of nanoparticles [29,30]. The particle size of as-prepared and recovered bulk and nano LSMO perovskite samples were given in Table 1. It is evident from that that the increase in particle size during temperature dependent ultrasonic velocity measurement due to further heating. The observed circular rings in the SAED (Fig. 6) pattern again confirms the crystalline nature of bulk and nano perovskite samples. The particle size of bulk and nano perovskite samples estimated from TEM images is given in Table 1 and agrees well with those obtained from SEM and XRD studies.

The BET surface area measurement for the bulk and nano perovskite samples was determined as 2.205 and 33.9 $m^2\,g^{-1}$, respectively. The higher surface area of nano perovskite samples compared with bulk perovskite samples ensures the fact that the catalytic activity of nano perovskites is higher than that of bulk perovskites [31]. The measured surface area and density of both bulk and nano perovskite samples were used to obtain the equivalent spherical diameter (D_{BET}) as shown in Table 1. The spherical diameter of nano perovskites was much lower (27 nm) than that of bulk perovskites (416 μm). Thus, the above findings from BET studies were in close agreement with those of earlier XRD studies.

The measured density of bulk and nano perovskite manganite materials are, respectively, 6543 and 6506 kg m^{-3}. The observed density reduction in nano perovskite samples may be ascribed to a decrease in the three-dimensional coordination of bonding in the grain boundaries of the nanocrystalline material and less stored dislocations [32,33]. The temperature dependence of longitudinal (L), shear (G), bulk (K), and Young's (E) modulus of bulk and nano perovskite samples are shown, respectively, in Figs. 7–10. A gradual decrease in moduli was observed in the temperature range of 300–366 K and 370–400 K for bulk perovskite samples, whereas in nano perovskite samples the above range of temperature changed slightly to 300–354 K (that is, it shifted to a lower temperature of 354 K from 366 K (for bulk samples)) and to 379–400 K (that is, it shifted to a higher temperature of 379 K from 370 K). However, an anomalous behaviour (that is, a sharp dip) was noticed at 368 K in the temperature range of 366–370 K (anomalous region) in bulk perovskite samples. In contrast, an anomalous behaviour was observed as a broad dip at 361 K in the

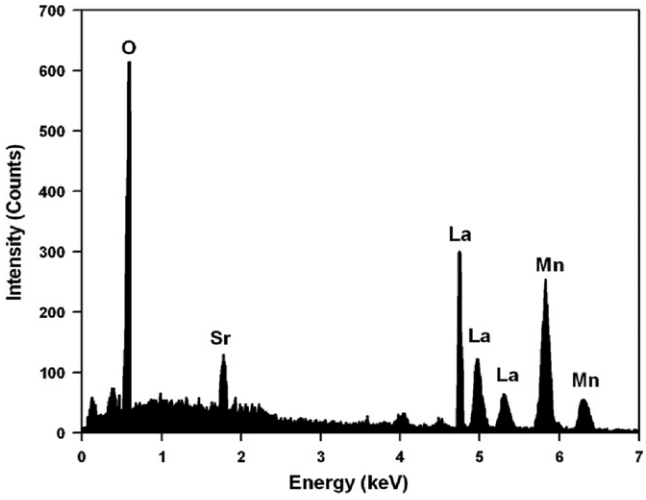

Elemental composition

Element	wt. %
La	0.61
Sr	0.39
Mn	1
O	2.99

Bulk LSMO sample

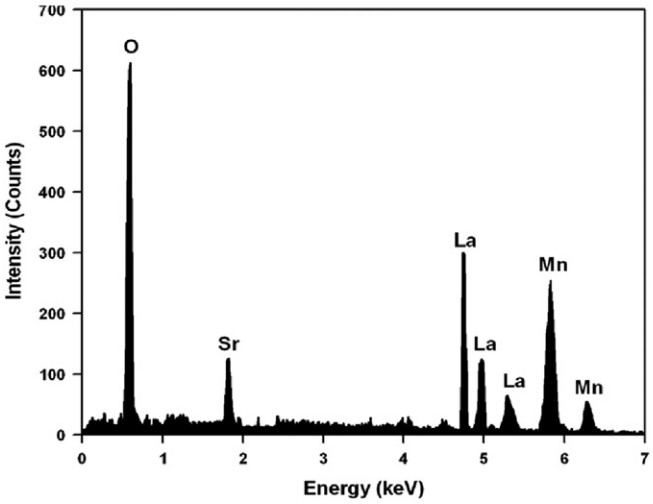

Elemental composition

Element	wt. %
La	0.615
Sr	0.395
Mn	1
O	3

Nano LSMO sample

Fig. 3. EDX pattern of bulk and nano $La_{0.61}Sr_{0.31}MnO_3$ perovskite manganite materials.

temperature range of 354–379 K (anomalous region) in nano perovskite samples.

On-line ultrasonic measurements and its derived parameters like elastic constants are powerful tools that help to obtain precise information about structural/phase transitions [34,35]. The increase in temperature of perovskites led to a monotonic decrease in elastic moduli during the absence of structural/phase transition. In contrast, an anomalous behaviour was noticed during the structural/phase transition, as reported in many systems [34–36]. Abrupt changes in the structural, spin, charge, and orbital degrees of freedom during the structural/phase transition were detected by ultrasonic measurement [20,34]. Hence, an anomalous behaviour was noticed at the structural/phase transition temperature. The observed dip in elastic modulus (Figs. 7–10) was used to explore the phase transition temperature of bulk and nano perovskite samples [34,37].

In present investigation, the anomalous obtained from the elastic moduli is correlated with phase diagram of $La_{1-x}Sr_xMnO_3$ perovskite materials obtained by the other studies like electrical, magnetic and Mossbauer [38–39]. The observed dip in elastic moduli at 368, and 361 K respectively for bulk and nano LSMO samples are correlated with the already reported phase transition temperature (phase diagram) for similar composition. Thus, the temperature at which the anomalous in velocities/attenuation is in agreement with phase transition temperature. Hence, the observed anomalous behaviour noticed in bulk and nano perovskites was due to the FM–PM transition in LSMO perovskites. Therefore, the observed anomalous behaviour with a sharp dip at 368 K for bulk samples and a broad dip at 361 K for nano perovskites is due to the FM–PM transition in LSMO perovskites. Temperatures 368 and 361 K are the FM–PM transition temperature, that is, the Curie temperature (T_C), of bulk and nano $La_{0.61}Sr_{0.39}MnO_3$ perovskite manganite samples.

It is clear that the T_C of nanostructured samples is lower than that of bulk perovskite samples. Another interesting observation to be noted from Figs. 7–10 is the fact that the anomalous region of nano perovskite samples is wider than that of bulk samples. Further, the amplitude of the dip in elastic moduli in nano perovskite is larger than that of bulk perovskites; that is, the observed FM–PM transition is sharp in bulk perovskite samples, whereas the transition is of broad nature (diffused) in nano perovskite samples. The decrease in T_C along with diffusion of

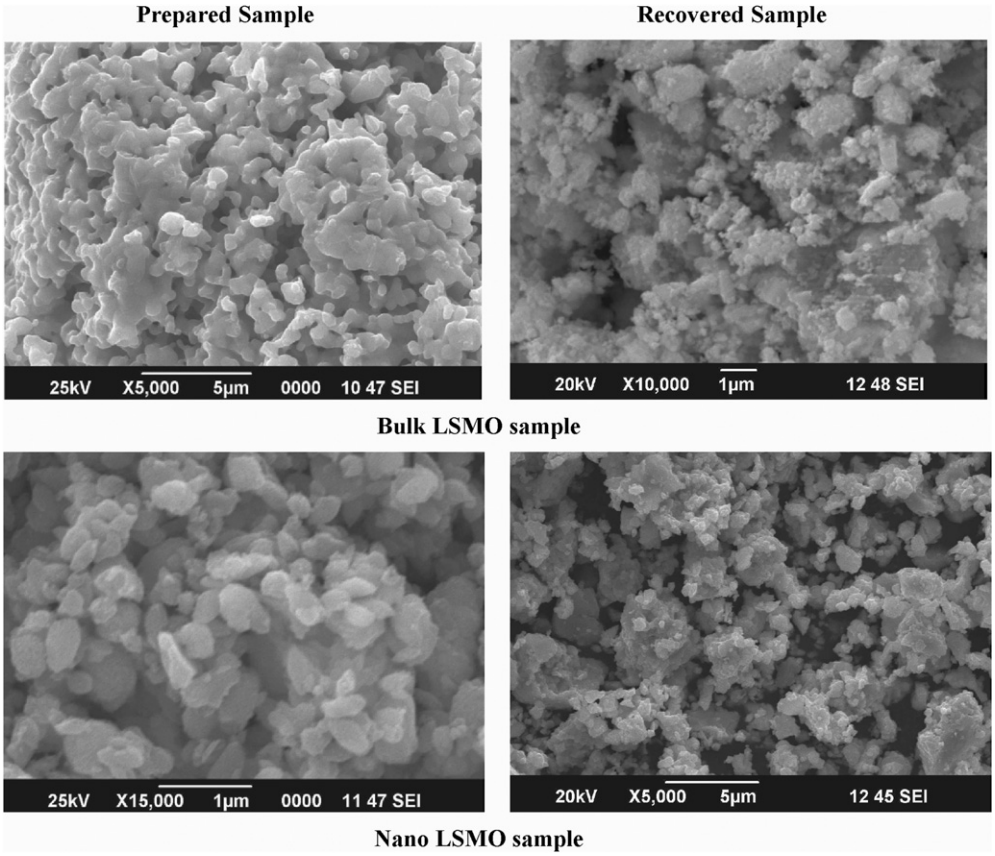

Fig. 4. TEM pattern of bulk and nano $La_{0.61}Sr_{0.31}MnO_3$ perovskite manganite materials.

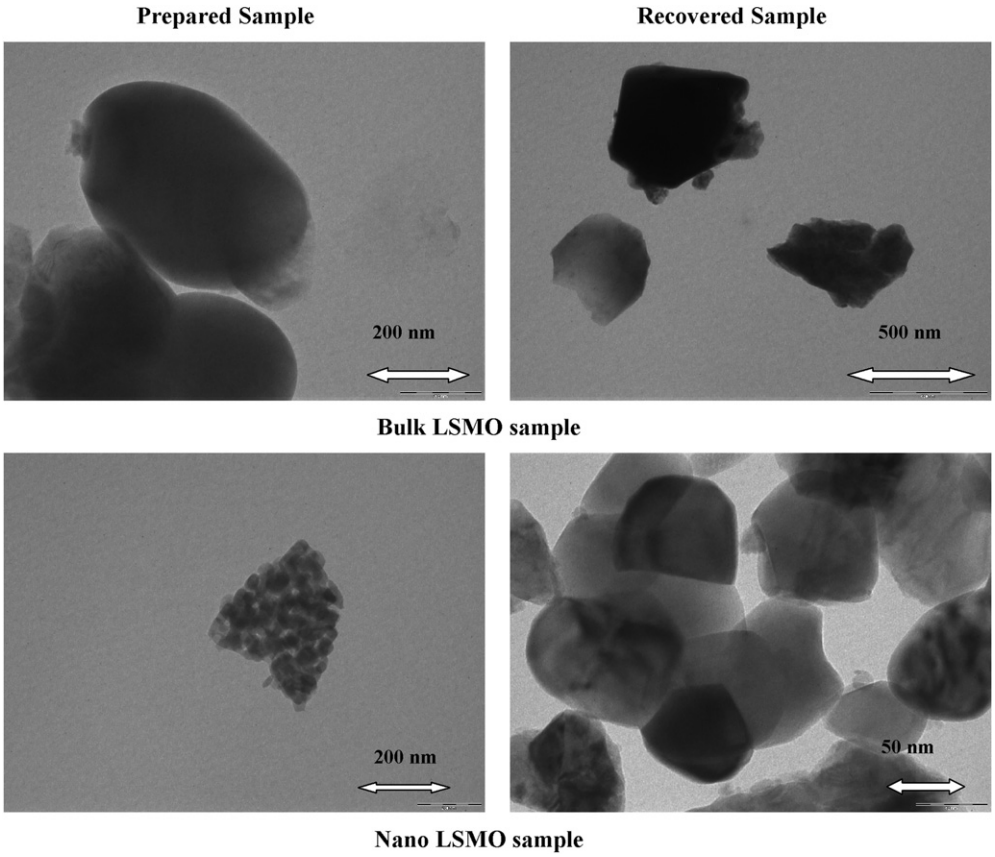

Fig. 5. TEM pattern of bulk and nano $La_{0.61}Sr_{0.31}MnO_3$ perovskite manganite materials.

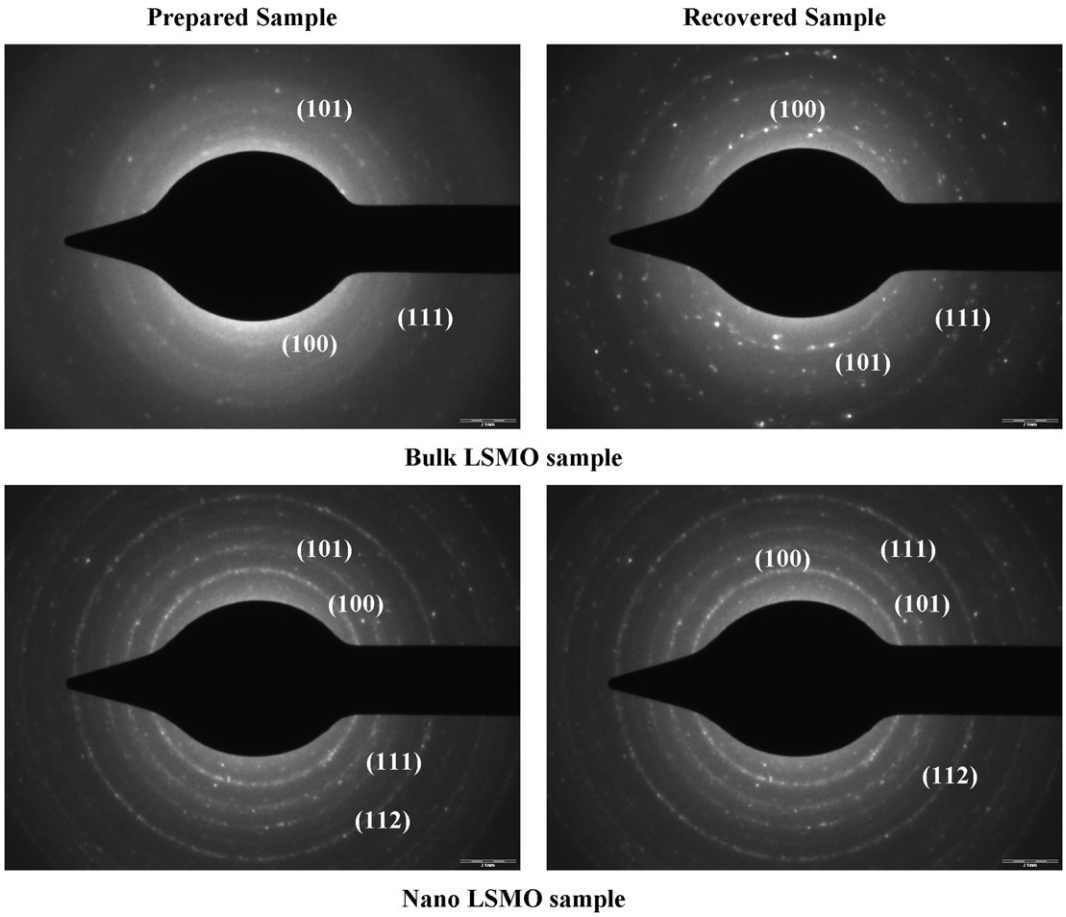

Fig. 6. SAED pattern of bulk and nano $La_{0.61}Sr_{0.31}MnO_3$ perovskite manganite materials.

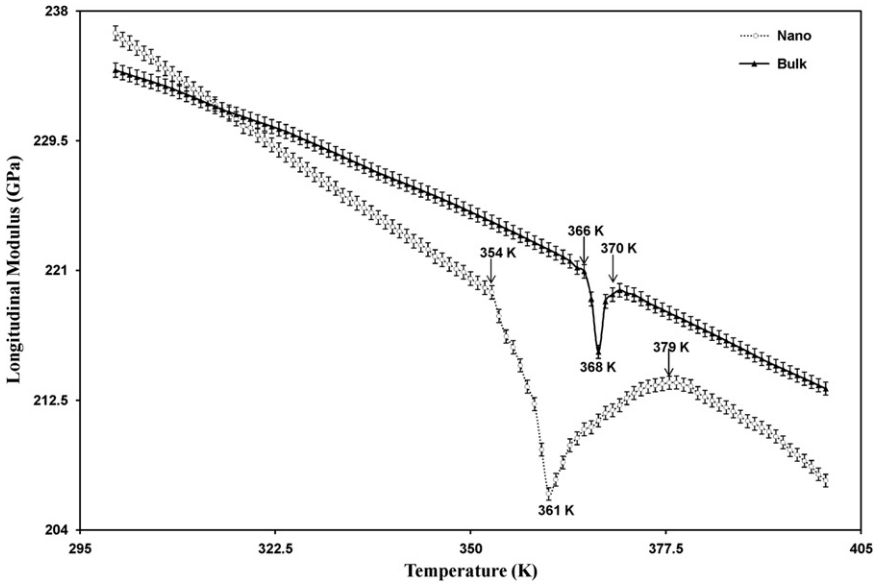

Fig. 7. Temperature dependence of longitudinal modulus of bulk and nano $La_{0.61}Sr_{0.31}MnO_3$ perovskite manganite materials.

the FM–PM phase transition may be correlated because of particle size effect.

When the size of the manganite grain is reduced to the nano range, the surface effects become more relevant to describe the structural and magnetic behaviour of the samples. The ferromagnetic spin fluctuations change to disordered spin fluctuations at T_C and subsequently lead to the PM state at Curie temperature. In LSMO nano particles, the surface disorder may be extended to a few layers into the interior of nano structured perovskites, which may prevent the formation of the long-range charge-ordered state. Hence, the charge-ordering (CO) transition is suppressed and diffused, and therefore the FM correlations could lead to an FM-ordered state at a lower temperature compared with the corresponding bulk perovskite sample. Similar observations for

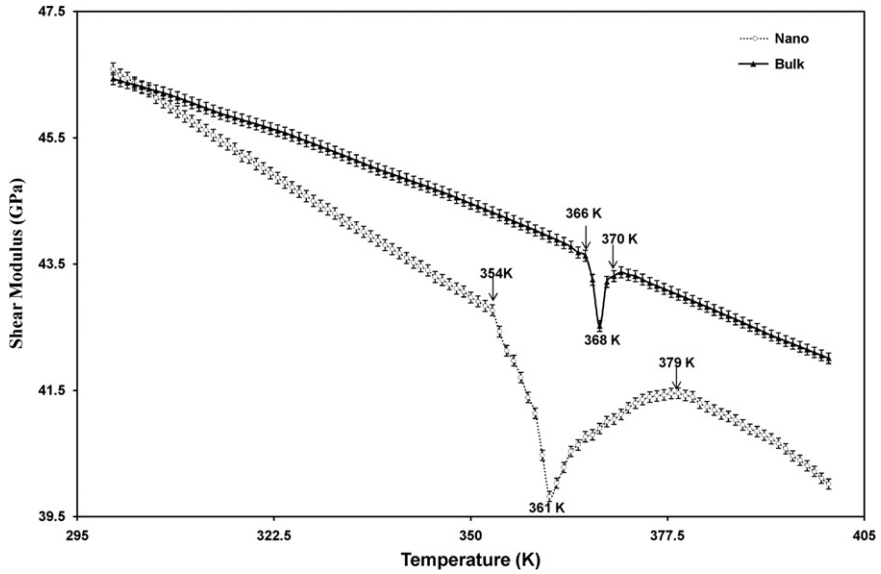

Fig. 8. Temperature dependence of shear modulus of bulk and nano $La_{0.61}Sr_{0.31}MnO_3$ perovskite manganite materials.

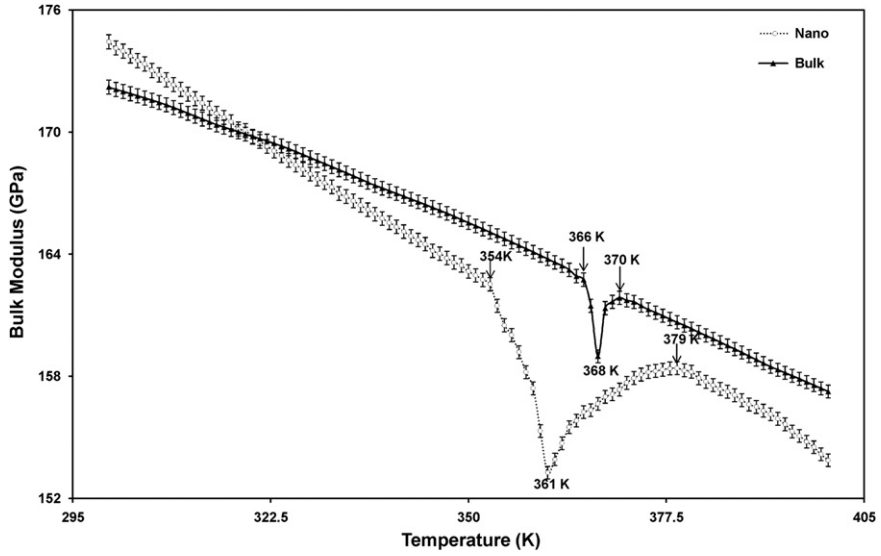

Fig. 9. Temperature dependence of bulk modulus of bulk and nano $La_{0.61}Sr_{0.39}MnO_3$ perovskite manganite materials.

low and absence of sharp transition have been revealed for nanostructured perovskite samples [20,36,40–42].

In the anomalous region (Figs.7–10), the elastic modulus started to decrease up to transition temperature (T_C) and then a gradual increase in elastic modulus was observed. Generally, the observed increase and decrease in modulus correlated, respectively, with the lattice softening and lattice hardening of the perovskite manganite materials [20,34,36]. The observed sharp/broad dip in transition temperature is due to the occurrence of the lattice hardening below T_C and lattice softening above T_C [20,36]. It is clear that the occurrence of lattice softening and hardening is more and wider in nano perovskites than in bulk samples because of the contribution from disordered surface layers, which plays an important role when particle size is reduced [15,42]. It is interesting to note that the peak broadening in ultrasonic studies at phase transition temperature is in line with the observation made from the XRD pattern for bulk and nanocrystalline samples. However, the observed amplitude of peak in the XRD pattern for bulk samples is higher than that of nano crystalline samples. The reverse trend is observed in ultrasonic studies, that is, higher peak amplitude for nano samples and smaller peak amplitude for bulk samples. The observed dip in elastic modulus was the key ingredient for the CMR properties of perovskite materials.

The observed broad peak in nanosamples is used to reveal the local distortion of the MnO_6 octahedral in perovskite samples [15,20,36,43], which plays an important role in determining the transport properties of perovskites. During the synthesis of nano perovskites, there may be many physical effects such as atomic disorder, contamination, reduction of atomic coordination and breaking of Mn–O–Mn bonds, termination of the crystal structure, and dislocation at the grain boundaries that may take place to a larger extent [43–45]. In perovskite manganite materials, the ferromagnetic double-exchange spin-spin coupling and super exchange interactions are very sensitive to the Mn–O–Mn bond angle and bond length. Therefore, the observed broad peak in nanostructured samples was used to confirm the enhanced local distortion of the MnO_6 octahedral in nanocrystalline perovskites

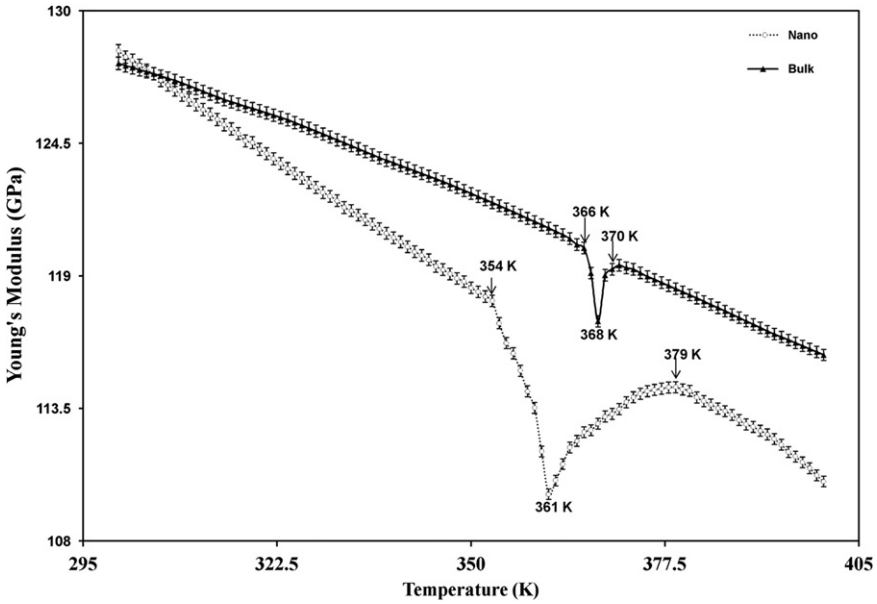

Fig. 10. Temperature dependence of Young's modulus of bulk and nano $La_{0.61}Sr_{0.39}MnO_3$ perovskite manganite materials.

during the FM–PM transition [20,36]. As a result, the enhanced charge and spin fluctuation is responsible for the observed reduction and diffusion of transition in nanostructured perovskites.

Further, the elastic modulus obtained through ultrasonic velocity measurement is used to reveal the magnetic interactions and coupling in LSMO perovskites. The linear magnetostriction effect is more dominant in LSMO perovskites than the volume magnetostriction effect, which is confirmed by the observed higher magnitude of L compared with G [20,46]. Linear (single ion) magnetostriction is responsible for the observed large variation in L and exists because of the strong spin–phonon interactions in LSMO perovskite manganite materials. If the magnetostriction is primarily due to volume magnetostriction, the anomalous behaviour in G will be absent [46]. Further, the observed softening and hardening in elastic moduli are due to the existence of strong electron–phonon coupling in LSMO perovskites [46]. The ultrasonic measurement on perovskites is used to indicate that the spin–phonon coupling is due to single-ion magnetostriction, whereas the electron–phonon coupling may originate from the dynamic Jahn–Teller effect [36,46]. Therefore, the observed results show direct evidence for electron–phonon and spin–phonon couplings at the phase transition temperature T_C in both bulk and nanostructured samples [20,46]. It is interesting to note that the magnitude of variation in the elastic moduli of nanostructured perovskite samples is wider than that of bulk perovskite samples. This shows that the coupling and interaction existing in perovskite manganite samples are enhanced when particle size is reduced. In all of the above, nanostructured perovskites take diffused FM–PM at lower temperature compared with bulk perovskites.

4. Conclusion

In the present investigation, bulk and nano $La_{0.61}Sr_{0.39}MnO_3$ perovskite manganite samples were prepared using solid-state reaction and sonochemical reactor methods. Characterisation studies confirm that the size of the bulk and nano perovskite samples were, respectively, 0.65 μm and 60 nm. On-line ultrasonic measurements on bulk and nano perovskite samples revealed that there is a shift in Curie temperature (T_C) from 368 to 361 K from bulk to nanoperovskite samples. The decrease in grain size led to a decrease in FM–PM transition of perovskites. Further, the observed broad nature of the decrease in T_C in the elastic modulus confirmed the absence of sharp FM–PM transition. The observed peak-broadening effect in elastic moduli at transition temperature was similar to the XRD pattern of nanocrystalline samples. Further, the observed anomalous behaviour both in longitudinal and shear modulus confirmed the fact that the linear magnetostriction effect was more dominant in bulk and nano perovskite manganite materials than the volume magnetostriction.

Acknowledgements

One of the authors (K.S) is thankful to Council of Scientific and Industrial Research (CSIR), New Delhi (8/570(0001)/2011dt.29.03.2011), for providing the senior research fellowship (SRF) to carry out this research.

References

[1] G. Lalitha, D. Das, D. Bahadur, P.Venugopal Reddy, J. Alloy Compd. 464 (2008) 6.
[2] I. Matos, S. Serio, M.E. Lopes, M.R. Nunes, M.E. Melo Jorge, J Alloy Compd. 509 (2011) 9617–9626.
[3] A.J. Millis, P.B. Littlewood, B.I. Shraiman, Phys. Rev. Letters 74 (1995) 5144–5147.
[4] P.-G. de Gennes, Phys. Rev. 118 (1960) 141–154.
[5] C.N.R. Rao, A.P.N. Santosh, A.K. Cheetham, Chem. Mater. 10 (1998) 2714–2722.
[6] R. Von Helmolt, J. Wecker, B. Holzapfel, L. Schultz, K. Samwer, Phys. Rev. Lett. 71 (1993) 2331.
[7] Clarence Zener, Phys. Rev. 82 (1951) 403–405.
[8] A.J. Campbell, G. Balakrishnan, M.R. Lees, D.McK. Paul, Phys. Rev. B 55 (14) (1977) 8622–8625.
[9] N. Dhahri, A. Dhahri, K. Cherif, J. Dhahri, K. Taibi, E. Dhahri, J. Alloy Compd. 496 (2010) 69–74.
[10] N. Zhang, W. Ding, W. Zhong, K. Du, K. Wang, Y. Du, Appl. Phys. A 65 (1997) 77–80.
[11] P. Shankar, P. Mandal, A.K. Bera, S.M. Yusuf, L.S. Sharath Chandra, V. Ganesan, Phys. Rev. B 78 (2008) 012415.
[12] Y. Luo, I. Szafraniak, N.D. Zakharov, V. Nagarajan, M. Steinhart, R.B. Wehrspohna, J.H. Wendorff, R. Ramesh, M. Alexe, Appl. Phys. Lett. 83 (2005) 440.
[13] B.I. Belevtsev, G.A. Zvyasina, K.R. Zhekov, I.G. Kolobov Panfilov, N.N. Galtsov, J. Fink, Finonicki, Appl. Phys. Lett. 88 (2006) 041920.

[14] Jessica R. Chocha, Pooja A. Chhelavda, J.A. Bhalodia, Trans. Indian Inst. Met. 64 (2011) 159–163.
[15] C.N.R. Rao, G.U. Kulkarni, P.J.P.P. Thomas, Edwards, Chem. Eur. J. 8 (2002) 28-35 8 (2002).
[16] S. Das, P. Chowdhury, T.K. Gundu Rao, D. Das, D. Bahadur, Solid State Commun. 121 (2002) 691–695.
[17] P. Kameli, H. Salamati, A. Aezami, J. Alloy Compd. 450 (2008) 7–11.
[18] Lide M. Rodriguez-Martinez, J. Paul Attfield, Phys. Rev. B 58 (1998) 2426–2429.
[19] S.S. Rao, S. Tripathi, D. Pandey, S.V. Bhat, Phys. Rev. B 74 (2006) 144416–144420.
[20] S. Sankar rajan, K. Sakthipandi, P. Manivasakan, V. Rajendran, Phase Transition 84 (2011) 657–672.
[21] K. Sakthipandi, V. Rajendran, T. Jayakumar and Baldev raj, J. Alloys. Compd., 512 (8), 3457–3467.
[22] A.L. Patterson, The Scherrer, Phys. Rev. 56 (1939) 978–982.
[23] B.R. Jennings, K. Parslow, Proc. R. Soc. Lond. A 419 (1988) 137–149.
[24] G. Lalitha, P. Venugopal Reddy, J. of Phys. Chem. Solids 70 (2009) 960–966.
[25] Genchu Tang, Yun Yu, Wei Chen, Yunzhen Cao, J. Alloy Compd. 461 (2008) 486–489.
[26] Sunita Keshri (Shaw), Leena Joshi, Sanjeeb Kumar Rout, J. Alloy Compd. 485 (2009) 501–506.
[27] V.S. Kolat, H. Gencer, M. Gunes, S. Atalay, Mater. Sci. Eng. B 140 (2007) 212–217.
[28] R.P. Sreekanth Chakradhar, B.M. Nagabhushana, G.T. Chandrappa, K.P. Ramesha, J.L. Rao, Mater. Chem. Phys. 95 (2006) 169–175.
[29] S. Daengsakul, C. Thomas, I. Thomas, C. Mongkolkachit, S. Siri, V. Amornkitbamrung, S. Maensiri, Nanoscale Res. Lett. 4 (2009) 839–845.
[30] R. Rajagopal, J. Mona, R.S. Joshee, S.N. Kale, S. Pradhan, A.B. Gaikwad, V. Ravi, Mater. Lett. 62 (2008) 1511–1513.
[31] W. Zhong, W. Chen, W.P. Ding, N. Zhang, A. Hu, Y.W. Du, Q.J. Yan, J. Magn. Magn. Mater. 195 (1999) 112–118.
[32] G. Lehmann, P. Hess, S. Weissmantel, G. Reisse, P. Scheible, A. Lunk, Appl. Phys. A 74 (2002) 41–45.
[33] T.D. Shen, Jianzhong Zhang, Yusheng Zhao, Acta Mater. 56 (2008) 3663–3671.
[34] Q.J. Huang, Y. Cheng, X.J. Liu, X.D. Xu, S.Y. Zhang, Ultrasonics 44 (2006) e1223–e1227.
[35] L. Godfrey, J. Philip, Solid State Commun. 97 (1996) 635–638.
[36] R.K. Zheng, C.F. Zhu, J.Q. Xie, R.X. Huang, X.G. Li, Mater. Chem. Phys. 75 (2002) 121–124.
[37] D.M. Hwang, Solid State Commun. 46 (1983) 177–181.
[38] Vincenzo Buscaglia Zhe Zhao, Maria Teresa Massimo Viviani, Liliana Buscaglia, Andrea Mitoseriu, Mats Testino, Mats Nygren, Johnsson, Paolo Nanni, Phys. Rev. B 70 (2004) 024107–024114.
[39] Mehran Rezaei, Majid Khajenoori, Behzad Nematollahi, Mat. Res. Bull. 46 (2011) 1632–1637.
[40] D.C. Krishna, P. Venugopal Reddy, J. Alloy Compd. 479 (2009) 661–669.
[41] K. Shantha Shankar, A.K. Raychaudhuri, J. Mater. Res. 21 (2006) 27–33.
[42] S.V. Trukhanov, A.V. Trukhanov, H. Szymczak, C.E. Botez, A. Adair, J. Low Temp. Phys. 149 (2007) 185–199.
[43] Sangita Bose, Pratap Raychaudhuri, Rajarshi Banerjee, Parinda Vasa, Pushan Ayyub, Mechanism of the size dependence of the superconducting transition of nanostructured Nb, Phys. Rev. Lett. 95 (2005) 147003–147006.
[44] T.L. Phan, S.G. Min, M.H. Phan, N.D. Ha, N. Chau, S.C. Yu, Phys. status solidi (b) 244 (2007) 1109–1117.
[45] R. Von Helmolt, J. Wecker, B. Holzapfel, L. Schultz, K. Samwer, Phys. Rev. Lett. 71 (1993) 2331–2333.
[46] Changfei Zhu, Renkui Zheng, Phys. Rev. B 59 (1999) 11169–11171.